25. Schubeler, D. *et al.* Genome-wide DNA replication profile for *Drosophila melanogaster*: a link between transcription and replication timing. *Nature Genet.* **32,** 438–442 (2002).
26. Zou, L. & Stillman, B. Assembly of a complex containing Cdc45p, replication protein A, and Mcm2p at replication origins controlled by S-phase cyclin-dependent kinases and Cdc7p-Dbf4p kinase. *Mol. Cell. Biol.* **20,** 3086–3096 (2000).

Supplementary Information accompanies the paper on **www.nature.com/nature**.

Acknowledgements We thank A. De Antoni, E. Schwob, S. Bell and J. Hegemann for the plasmids; K. Tamai for the special preparation of BrdU antibody; H. Araki, K. Okumura, E. Winzeler, M Foiani, T. Yada and K. Umezu for their comments; E. Schwob, F. Uhlmann, R. Cha and H. Yoshikawa for critical reading of the manuscript; T. Itoh, Y. Nakao, A. Nakada and C. Kawagoe for technical assistance; and Y. Sakaki and all the members of the Genome Structure and Function team for their support. This work was supported partly by grants-in-aid on priority areas from the Ministry of Education, Culture, Sports, Science and Technology, Japan, to K.S. Y. Katou is a Junior Research Associate of the RIKEN GSC.

Competing interests statement The authors declare that they have no competing financial interests.

Correspondence and requests for materials should be addressed to K.S. (shirahi@gsc.riken.go.jp). Data presented in this paper can be obtained from GEO (http://www.ncbi.nlm.nih.gov/geo) with accession number GSE486.

Replication of a *cis–syn* thymine dimer at atomic resolution

Hong Ling[1], François Boudsocq[2]*, Brian S. Plosky[2], Roger Woodgate[2] & Wei Yang[1]

[1]*Laboratory of Molecular Biology, National Institute of Diabetes and Digestive and Kidney Diseases, and* [2]*Laboratory of Genomic Integrity, National Institute of Child Health and Human Development, National Institutes of Health, Bethesda, Maryland 20892, USA*

* Present address: Institut de Pharmacologie et de Biologie Structurale, CNRS, 31077 Toulouse, France

Ultraviolet light damages DNA by catalysing covalent bond formation between adjacent pyrimidines, generating *cis–syn* cyclobutane pyrimidine dimers (CPDs) as the most common lesion[1]. CPDs block DNA replication by high-fidelity DNA polymerases, but they can be efficiently bypassed by the Y-family DNA polymerase pol η[2,3]. Mutations in *POLH* encoding pol η are implicated in nearly 20% of xeroderma pigmentosum, a human disease characterized by extreme sensitivity to sunlight and predisposition to skin cancer[4–6]. Here we have determined two crystal structures of Dpo4, an archaeal pol η homologue, complexed with CPD-containing DNA, where the 3′ and 5′ thymine of the CPD separately serves as a templating base. The 3′ thymine of the CPD forms a Watson–Crick base pair with the incoming dideoxyATP, but the 5′ thymine forms a Hoogsteen base pair with the dideoxyATP in *syn* conformation. Dpo4 retains a similar tertiary structure, but each unusual DNA structure is individually fitted into the active site for catalysis. A model of the pol η–CPD complex built from the crystal structures of *Saccharomyces cerevisiae apo*-pol η and the Dpo4–CPD complex suggests unique features that allow pol η to efficiently bypass CPDs.

From bacteria to humans, most ultraviolet-induced photoproducts are removed by well-characterized DNA repair mechanisms[7]. Photoproducts remaining during DNA replication are either avoided by recombination-dependent template switching or bypassed by specialized low-fidelity polymerases that can synthesize DNA directly opposite lesions[8]. Crystal structures of three Y-family polymerases[9,10], including a large fragment of *S. cerevisiae* pol η and two archaeal DinB homologues, Dbh and Dpo4 from *Sulfolobus solfataricus*, revealed a right-hand-like catalytic core composed of palm, thumb and finger domains as found in all DNA polymerases, and a unique little finger domain at the carboxy terminus. In the ternary complex of Dpo4, primer-template and an incoming nucleotide, the thumb and little finger domains hold the DNA duplex, and the active site formed between the palm and finger domains is spacious and solvent-accessible owing to the unusually small thumb and finger domains[11].

Dpo4 exhibits robust polymerase activity on undamaged DNA and can by-pass a variety of DNA lesions, including CPDs[12]. By adjusting the register of the 3′ end of the primer strand opposite a CPD-containing template and using dideoxyATP (ddATP) to reduce nucleotidyl transfer, we have crystallized Dpo4 with the 3′ (TT-1) or 5′ (TT-2) thymine of the CPD base-paired with ddATP and poised for DNA synthesis (Fig. 1). These co-crystal structures of Dpo4 and CPD-containing DNA, determined at 2.3 Å and 2.0 Å resolution (Table 1), provide the first glimpse of how a DNA polymerase replicates severely distorted DNA.

The Dpo4 structures in TT-1 and TT-2 are nearly identical except for a less than 1 Å shift of the little finger domain, which is probably due to differences in the local structure of the DNA as well as different crystal lattice contacts (Fig. 1 and Table 1). Compared with the structure of Dpo4 complexed with undamaged DNA in the same space group as TT-1 (ref. 11), the thumb and little finger domains in both TT-1 and TT-2 move by 1-2 Å leading to a concomitant shift of the DNA duplex (Supplementary section 1). Notably, this movement of protein and DNA appears to pivot around the catalytic carboxylate triad and results in a similar arrangement of DNA substrate in the active site regardless of the nature of the templating base (Fig. 1e). The three catalytic carboxylates—Asp 7, Asp 105 and Glu 106—and the two metal ions are superimposable in TT-1 and TT-2 (Fig. 1c). Although the DNA duplex and the ddATP are shifted, the 3′ OH group of the primer strand remains within 4 Å of the α-phosphate of the incoming nucleotide.

A covalently linked thymine dimer imposes severe steric hindrance on DNA polymerases. For the A- and B-family DNA polymerases, only one templating base is accommodated in the active site for each cycle of primer extension and the adjacent 5′ base is flipped out[13]. Covalently linked CPDs cannot separate and therefore do not fit into the 'closed-off' active site of replicative polymerases. In contrast, when the 3′ base of the thymine dimer serves as a template in TT-1, the entire CPD slips into the open active site of Dpo4 (Fig. 1c, d). The 3′ thymine and the incoming ddATP, although not perfectly co-planar, form two Watson–Crick-type hydrogen bonds of 2.6–2.7 Å in length (Fig. 2). The 5′ thymine of the CPD is only 2.7 Å away from the carbonyl oxygen of Gly 58. This glycine residue is replaced by Ser or Met in human and *S. cerevisiae* pol η. Although the Met or Ser side chain points towards the major groove and neither would clash with DNA (Fig. 3), Gly is

Table 1 **Summary of crystallographic data**

Crystal (space group)	TT-1 ($P2_12_12$)	TT-2 ($P2_12_12_1$)
Unit cell (*a*, *b*, *c*) (Å)	98.5, 101.6, 52.2	98.7, 102.3, 106.1
Number of complexes in AU	1	2
Non-hydrogen atoms	3,569	7,494
Resolution range (Å)†	19.34–2.28 (2.32–2.28)	19.9–2.00 (2.06–2.03)
R_{merge}*†	0.070 (0.554)	0.044 (0.492)
Unique reflections	24,302	69,785
Completeness (%)†	98.9 (99.0)	99.4 (95.0)
R-value‡	0.252	0.222
R_{free}§	0.282 (684 reflections)	0.256 (1,012 reflections)
r.m.s. deviation bond length (Å)	0.009	0.010
r.m.s. deviation bond angle (°)	1.72	1.70
Average *B*-value (Wilson; Å^2)	61.6 (66.5)	46.2 (43.1)

r.m.s., root mean square. AU, asymmetric units.
*$R_{merge} = \sum_h \sum_i |I_{hi} - \langle I_h \rangle| / \sum \langle I_h \rangle$, where I_{hi} is the intensity of the *i*th observation of reflection *h*, and $\langle I_h \rangle$ is the average intensity of redundant measurements of the *h* reflections.
†Data of the highest resolution shell are shown in parentheses.
‡*R*-value $= \sum ||F_o| - |F_c|| / \sum |F_o|$, where F_o and F_c are the observed and calculated structure-factor amplitudes.
§R_{free} is monitored with the reflections in parentheses excluded from refinement.

less restricted in backbone conformation and thus more accommodating for the CPD. Indeed, replacing the equivalent Ser 62 in human pol η by Gly made the mutant polymerase bypass a CPD more efficiently[14].

In TT-2, the 3′ thymine of the CPD forms a canonical Watson–Crick base pair with the adenine at the 3′ end of the primer strand, and the 5′ thymine is opposite the incoming ddATP. The templating thymine constrained by the inter-base covalent bonds, however, does not rotate 36° or rise by 3.4 Å relative to the preceding base pair as in normal DNA. If ddATP assumes its usual conformation for nucleotidyl transfer, it could not form a Watson–Crick base pair with the 5′ thymine of the CPD. If it were to form the base pair, the triphosphate could not fit into its binding site for the chemical reaction. In TT-2, the incoming ddATP assumes a *syn* conformation

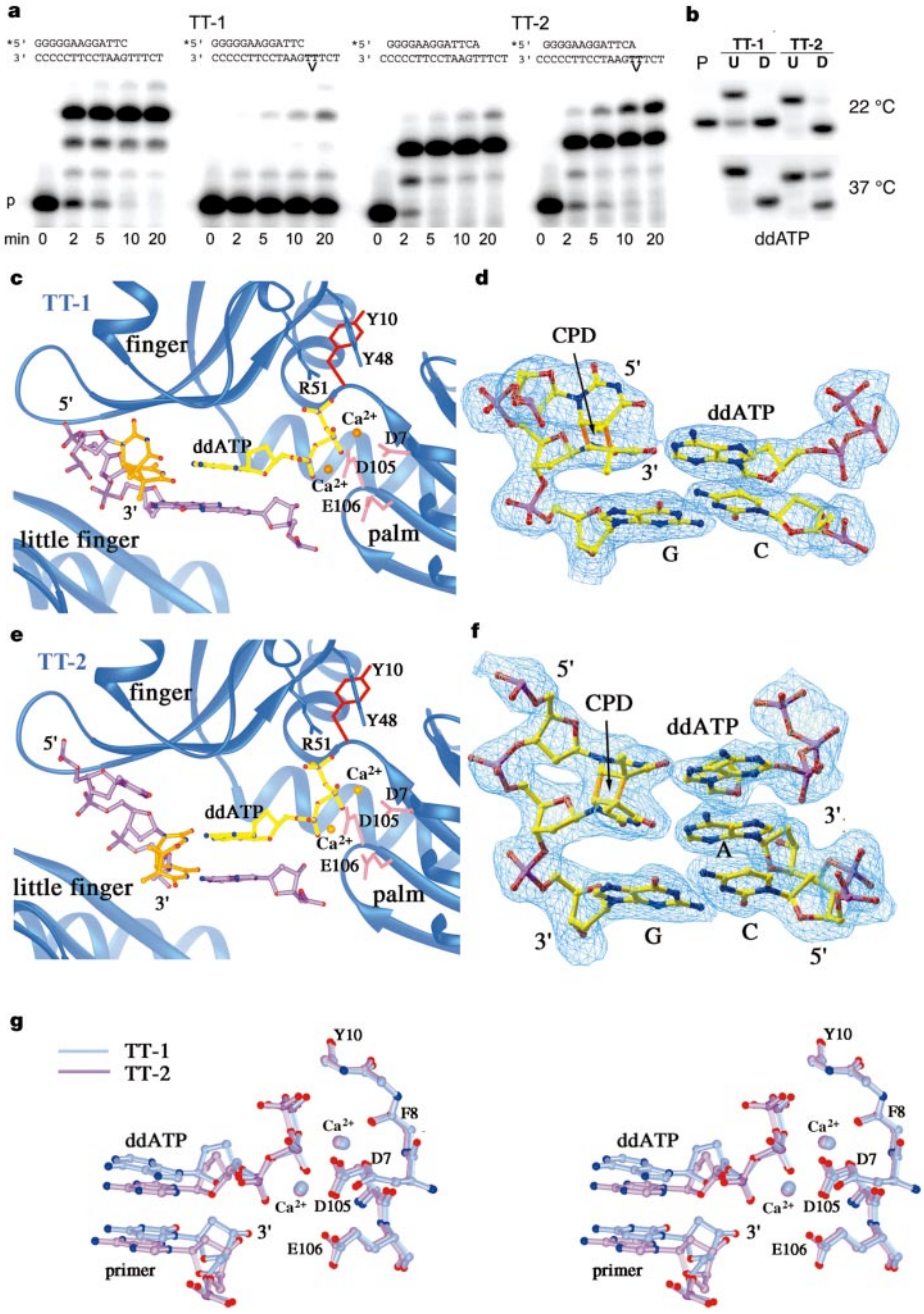

Figure 1 Replication of a CPD by Dpo4 in solution and crystals. **a**, Extension of two primers (13 nucleotides each) paired with undamaged or CPD-containing 18-nucleotide templates used in the crystallization studies (TT-1, TT-2). Reactions were carried out with 10 nM DNA substrate, 10 nM Dpo4 and 100 μM dATP at 37 °C for 2, 5, 10 or 20 min. **b**, Inhibition of primer extension by ddATP. P indicates primer strand, and U and D indicate undamaged and CPD-containing template, respectively. The reactions took place for 30 min at 22 °C or 37 °C as indicated. **c**, The active site of TT-1, where the 3′ thymine of the CPD (orange) is base-paired with ddATP (yellow). The conserved residues interacting with ddATP and catalytic carboxylates are highlighted. Tyr 10, which immobilizes the finger domain by wedging between the palm and finger domains, is shown in red. **d**, Replication at the 3′ T of the CPD. The CPD and the replicating and preceding base pairs of TT-1 are shown with the $F_o - F_c$ omit electron densities. **e**, Active site of TT-2, where the 5′ thymine of the CPD is base-paired with ddATP, **f**, The replicating and two preceding base pairs of the TT-2 are shown with the $F_o - F_c$ omit electron densities. **g**, Stereo view of the TT-1 (blue) and TT-2 (pink) active-site superposition. The three catalytic carboxylates, two Ca^{2+} ions, the 3′ nucleotide of the primer strand, and the incoming nucleotide are shown in the ball-and-stick model.

and forms a Hoogsteen base pair with the 5′ thymine of the CPD, thereby maintaining the triphosphate contact with Dpo4 for nucleotidyl transfer (Fig. 1e, f and 2c). In the absence of the 3′ OH of ddATP, the chemical bond does not form in the TT-2 crystal nor in solution at 22 °C (Fig. 1b). At 37 °C, incorporation of ddAMP opposite the 5′ T of the CPD is much improved (Fig. 1b), and with dATP Dpo4 bypasses the 5′ T of the CPD as efficiently as it does with undamaged DNA (Fig. 1a).

Hoogsteen base-pairing in duplex DNA has been observed when DNA is unwound or bound with intercalating drugs[15], and occasionally when DNA is distorted by protein[16–18]. In the crystal structure of a CPD-containing oligonucleotide[19], Watson–Crick base pairs were retained, but the hydrogen bonds at the 5′ T of the CPD were weakened and the DNA backbone of the strand opposite the CPD was distorted (Fig. 2a). To avoid backbone distortion, the Hoogsteen base pair at the 5′ T of a CPD is probably favoured by all DNA polymerases for catalysis, which we believe is the first example of a Hoogsteen base pair facilitating an enzymatic reaction.

T to C and T to A mutations are observed at the 3′ T of a CPD due to misincorporation of dGMP or dTMP, yet mutations rarely occur at the 5′ T (refs 20, 21). When the 3′ T of the CPD serves as a template, the close contact between the 5′ T and the polymerase induces a 3 Å shift of the CPD towards the major groove, thus leaving ample space for the 3′ T to form a wobble base pair with dGTP or dTTP, with each making two hydrogen bonds. At the 5′ T of the CPD, however, the restraint imposed by the Hoogsteen base pair discriminates against guanine and pyrimidines, and only adenine, which makes two hydrogen bonds with thymine either by Watson–Crick or Hoogsteen base-pairing, is acceptable.

Dpo4 is rather inefficient at replicating the 3′ T of a CPD (Fig. 1a), whereas pol η replicates past CPDs as efficiently as undamaged DNA[2,3]. To uncover the molecular basis for efficient bypass of CPDs by pol η, we generated a model of pol η complexed with a CPD based on TT-1 and the *S. cerevisiae* pol η structure[22]. With the TT-1 structure held fixed, pol η was brought in by superposition of its most conserved palm domain with that of Dpo4 (Fig. 3a). The finger, thumb and little finger domains of pol η, which bear many similarities to the corresponding domains of Dpo4, apparently need to rotate 16°, 16° and 45°, respectively, to be in position to interact with the DNA as the domains of Dpo4 do in TT-1 (Fig. 3a). In this modelled complex, pol η undergoes a 'closing' motion and makes numerous favourable contacts with the DNA. Even the Hoogsteen base pair fits well in the modelled pol η, when the TT-2 structure is superimposed onto TT-1.

Kinetic studies have suggested that pol η undergoes an induced-fit conformational change[23]. Movement of the finger domain upon substrate binding is universal among the A- and B-family polymerases and is thought to be crucial for high-fidelity DNA replication[13]. Although conformational change of the finger domain in response to substrate binding has not been observed in the Dpo4 and Dbh structures[10,24,25], our model clearly indicates an induced fit of the finger, thumb and little finger domains in pol η. The finger domain is closest to the replicating base pair and participates in the active-site formation; therefore its movement is most significant.

Structure-based sequence alignment suggests that several amino acid substitutions in human and yeast pol η make their active sites much less exposed to solvent than that of Dpo4 (Fig. 3). The larger Gln and Ile side chains in place of Dpo4's Val 32 and Ala 44 potentially interact with the minor groove of the replicating base

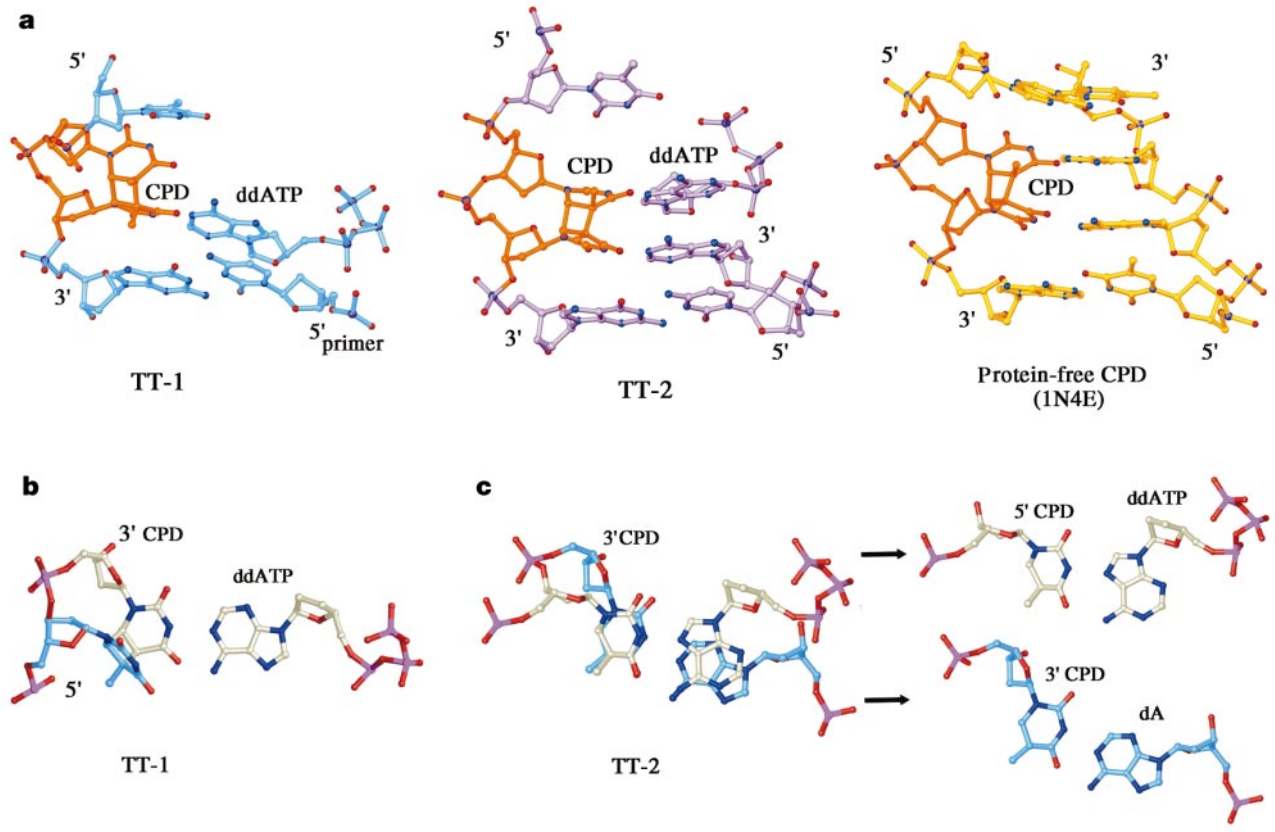

Figure 2 Structural comparison of the CPD complexed with Dpo4 and protein free. **a**, Structures of the CPD (orange) and surrounding nucleic acids in TT-1 (blue), TT-2 (pink) and in the absence of protein (yellow)[19] are shown in the ball-and-stick model after superposition of the CPDs. **b**, **c**, Ball-and-stick presentations of base-pairing of the CPDs in TT-1 (**b**) and TT-2 (**c**). The phosphorus atoms are shown in purple, oxygen in red and nitrogen in dark blue. The carbon atoms of the replicating base pair are white, and others are light blue.

pair and stabilize the CPD. The side chain of the Met or Ser that replaces Gly 58 of Dpo4 extends the protein–DNA interactions into the major groove. The Arg in place of Ala 57 of Dpo4 potentially orients the incoming nucleotide by charge interactions with the β-phosphate, and the aliphatic portion of this Arg shields the major groove of the replicating base pair and the triphosphate moiety of the incoming nucleotide. Because of these amino acid substitutions in pol η, incoming nucleotides cannot enter the closed active site.

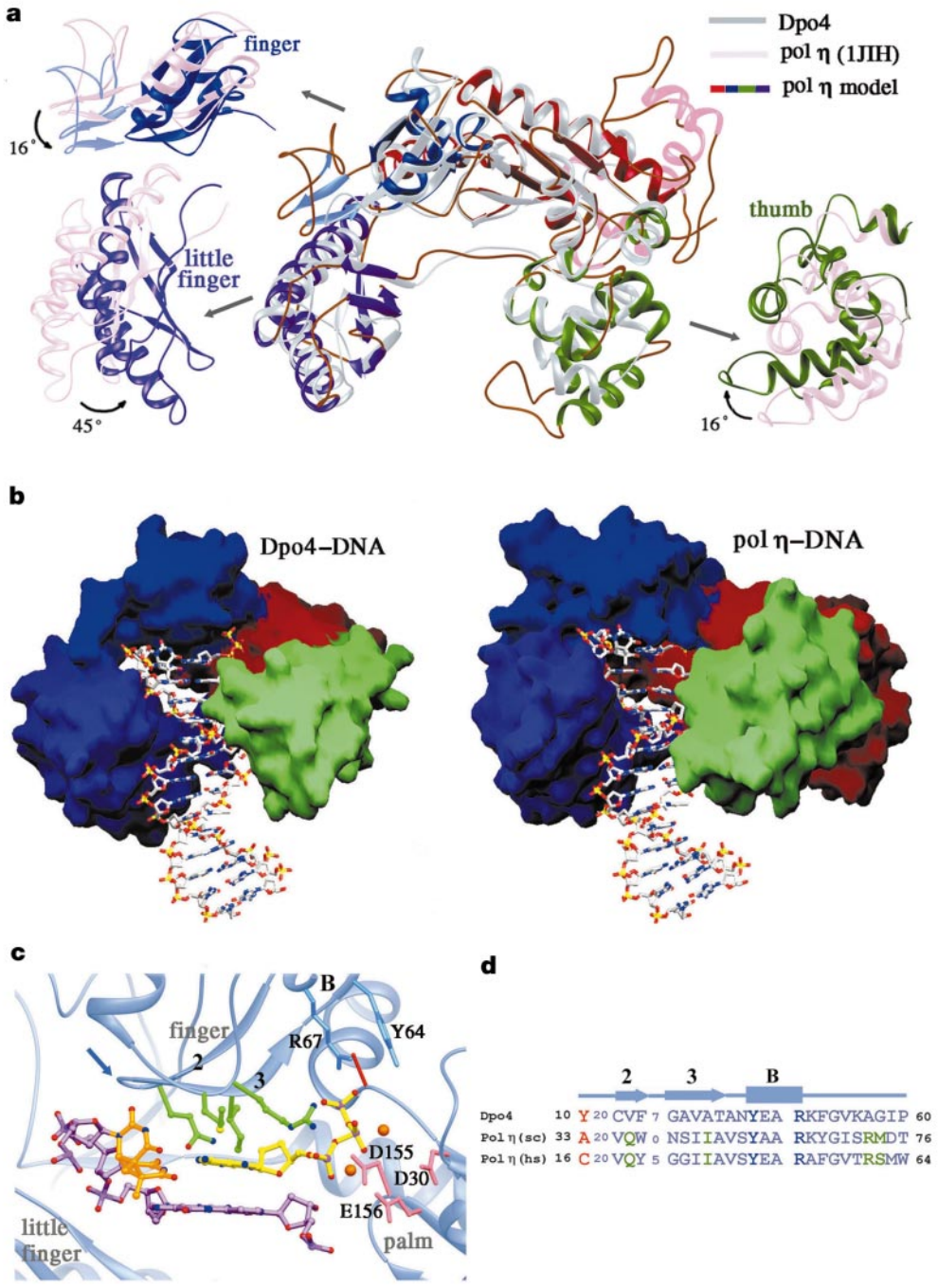

Figure 3 Modelling of *S. cerevisiae* pol η complexed with a CPD. **a**, Superposition of pol η (multicoloured) and Dpo4 (grey) after individual rigid-body movements of the pol η thumb, finger and little finger domains. Movements of the pol η domains between the *apo*-protein crystal structure (light pink) and the composite model are depicted in the surrounding panels. The pol η palm, thumb, finger and little finger domain are coloured red, green, blue and purple, respectively. The insertions unique in the pol η palm and finger domains are shown in pink and light blue. **b**, Comparison of the Dpo4 TT-1 crystal structure and the pol η–CPD model. The proteins are shown in molecular surface, and each domain is colour-coded as pol η in **a**. DNA and the incoming nucleotide are represented as stick models. The template and the incoming nucleotide in the pol η complex are less solvent-accessible than those complexed with Dpo4. **c**, Close-up of the pol η active site. Pol η is shown as the light-blue ribbon diagram; the DNA substrate, the conserved protein residues and the two divalent cations are coloured as in Fig. 1c, e. Amino acid substitutions in human and *S. cerevisiae* pol η, which may enhance the efficiency for bypass of CPD, are highlighted in green. Ala 33 is highlighted in red. The blue arrow points out the deletion between β-strands 1 and 2 in pol η. **d**, Sequence alignment of the residues in finger domains of Dpo4, *S. cerevisiae* and human pol η that interact with the replicating base pair. The conserved residues are colour-coded as in **c**. The numbers in black are the beginning and ending residue numbers of each sequence; the numbers in blue indicate the intervening residues omitted in the alignment.

To open up the finger domain between successive rounds of polymerization, Tyr 10 of Dpo4, which immobilizes the finger domain by wedging between the palm and finger domains (Fig. 1), is replaced by Ala or Cys in pol η (Fig. 3d). The solvent-occluded active site together with the conformational change from the open DNA-free to closed DNA-bound form may, therefore, facilitate the ability of pol η to bypass CPDs. □

Methods

Preparation of protein and DNA

Dpo4 was prepared as reported previously[11]. An 18-nucleotide DNA oligonucleotide (3′-CCCCCTTCCTAAG**TT**TCT-5′) containing a *cis–syn* thymine dimer (in bold) at the 14th and 15th positions from the 3′ end was chemically synthesized and purified by Glen Research. Two complementary 13-nucleotide primer strands were purchased from Oligo Etc. Primer-1 (5′-GGGGGAAGGATTC-3′) base-paired with the first 13 bases of the CPD-containing template, and primer-2 (5′-GGGGAAGGATTCA-3′) base-paired with the 2nd to 14th bases of the template including the 3′ thymine of the CPD. The template and primer strands were annealed and mixed with purified Dpo4 at a molar ratio of 1.2:1. The final concentration of Dpo4 was 6 mg ml^{-1} in a buffer of 20 mM HEPES (pH 7.0), 5 mM $MgCl_2$ and 150 mM NaCl.

Crystallization and structure determination

The TT-1 crystal with primer-1 was grown using the hanging-drop method with 15% PEG3350, 0.2 M calcium acetate, 2.5% glycerol at 20 °C after mixing the protein–DNA sample with 1 mM ddATP for 10 min at 22 °C before setting up the drop. The TT-2 crystal with primer-2 was grown similarly. Macroseeding was performed a couple of times to enlarge crystals. Crystals were flash-frozen in propane equilibrated with liquid nitrogen for storage and data collection. Diffraction data were collected using a Raxis IV mounted on a Rigaku RU200 generator and processed using HKL[26]. The TT-1 crystal was isomorphous to the original Dpo4–DNA complex (space group $P2_12_12$), but the TT-2 crystal was in $P2_12_12_1$ space group and had two Dpo4–DNA complexes in each asymmetric unit (Table 1).

Both crystal structures were solved by molecular replacement[27] using the original Dpo4–DNA complex as a search model, and refined to 2.03 and 2.28 Å resolution, respectively[27,28] (Table 1). The topology and parameter data of the CPD for refinement was generated from 1VAS[29]. All protein residues are in the most favoured and allowed region of a Ramachandran plot.

Model building

Pol η was modelled onto the TT-1 structure by superimposing the palm domains of the two proteins[30]. The other three domains were each adjusted as a rigid body to optimize their superposition with the Dpo4 structure. Superposition of the thumb domains was approximate owing to multiple insertions in yeast pol η. After adjusting a few side-chain torsion angles guided by the rotamer library, the resulting model of the pol η–DNA complex has no steric clashes, and pol η is transformed from an open DNA-free state to a closed DNA-bound conformation.

In vitro bypass of CPDs by Dpo4

The 5′ [^{32}P]-labelled 13-nucleotide primers and unlabelled 18-nulceotide template, as described in the crystallization studies, as well as an undamaged 18-nucleotide template were annealed at a molar ratio of 1:2. Standard replication reactions of 10 μl contained 40 mM Tris-HCl at pH 8.0, 5 mM $MgCl_2$, 100 μM of ultrapure dATP or ddATP (Amersham Pharmacia Biotech), 10 mM DTT, 250 μg ml^{-1} BSA, 2.5% glycerol, 10 nM 5′ [^{32}P] primer-template DNA and 10 nM Dpo4. After incubation at 37 °C or 22 °C, reactions were terminated by the addition of 10 μl of 95% formamide/10 mM EDTA and the samples heated to 100 °C for 5 min. Reaction mixtures (5 μl) were subjected to 20% polyacrylamide/7 M urea gel electrophoresis and replication products visualized by PhosphorImager analysis.

Received 10 June; accepted 22 July 2003; doi:10.1038/nature01919.
Published online 6 August 2003.

1. Ravanat, J. L., Douki, T. & Cadet, J. Direct and indirect effects of UV radiation on DNA and its components. *J. Photochem. Photobiol. B* **63,** 88–102 (2001).
2. Masutani, C., Kusumoto, R., Iwai, S. & Hanaoka, F. Mechanisms of accurate translesion synthesis by human DNA polymerase η. *EMBO J.* **19,** 3100–3109 (2000).
3. Johnson, R. E., Washington, M. T., Prakash, S. & Prakash, L. Fidelity of human DNA polymerase η. *J. Biol. Chem.* **275,** 7447–7450 (2000).
4. Lehmann, A. R. Replication of damaged DNA in mammalian cells: new solutions to an old problem. *Mutat. Res.* **509,** 23–34 (2002).
5. Masutani, C. *et al.* The *XPV* (xeroderma pigmentosum variant) gene encodes human DNA polymerase η. *Nature* **399,** 700–704 (1999).
6. Johnson, R. E., Kondratick, C. M., Prakash, S. & Prakash, L. *hRAD30* mutations in the variant form of xeroderma pigmentosum. *Science* **285,** 263–265 (1999).
7. Thoma, F. Light and dark in chromatin repair: repair of UV-induced DNA lesions by photolyase and nucleotide excision repair. *EMBO J.* **18,** 6585–6598 (1999).
8. Hoeijmakers, J. H. Genome maintenance mechanisms for preventing cancer. *Nature* **411,** 366–374 (2001).
9. Ohmori, H. *et al.* The Y-family of DNA polymerases. *Mol. Cell* **8,** 7–8 (2001).
10. Yang, W. Damage repair DNA polymerases Y. *Curr. Opin. Struct. Biol.* **13,** 23–30 (2003).
11. Ling, H., Boudsocq, F., Woodgate, R. & Yang, W. Crystal structure of a Y-family DNA polymerase in action: a mechanism for error-prone and lesion-bypass replication. *Cell* **107,** 91–102 (2001).
12. Boudsocq, F., Iwai, S., Hanaoka, F. & Woodgate, R. *Sulfolobus solfataricus* P2 DNA polymerase IV (Dpo4): an archaeal DNA polymerase with properties akin to eukaryotic Pol η. *Nucleic Acids Res.* **29,** 4607–4616 (2001).
13. Patel, P. H., Suzuki, M., Adman, E., Shinkai, A. & Loeb, L. A. Prokaryotic DNA polymerase I: evolution, structure, and "base flipping" mechanism for nucleotide selection. *J. Mol. Biol.* **308,** 823–837 (2001).
14. Glick, E., Vigna, K. L. & Loeb, L. A. Mutations in human DNA polymerase η motif II alter bypass of DNA lesions. *EMBO J.* **20,** 7303–7312 (2001).
15. Park, J. Y. & Choi, B. S. NMR investigation of echinomycin binding to d(ACGTTAACGT)2: Hoogsteen versus Watson-Crick A.T base pairing between echinomycin binding sites. *J. Biochem. (Tokyo)* **118,** 989–995 (1995).
16. Aishima, J. *et al.* A Hoogsteen base pair embedded in undistorted B-DNA. *Nucleic Acids Res.* **30,** 5244–5252 (2002).
17. Patikoglou, G. A. *et al.* TATA element recognition by the TATA box-binding protein has been conserved throughout evolution. *Genes Dev.* **13,** 3217–3230 (1999).
18. Bunting, K. A. *et al.* Crystal structure of the *Escherichia coli dcm* very-short-patch DNA repair endonuclease bound to its reaction product-site in a DNA superhelix. *Nucleic Acids Res.* **31,** 1633–1639 (2003).
19. Park, H. *et al.* Crystal structure of a DNA decamer containing a *cis–syn* thymine dimer. *Proc. Natl Acad. Sci. USA* **99,** 15965–15970 (2002).
20. Zhang, H. & Siede, W. UV-induced T → C transition at a TT photoproduct site is dependent on *Saccharomyces cerevisiae* polymerase η *in vivo*. *Nucleic Acids Res.* **30,** 1262–1267 (2002).
21. Szekeres, E. S. Jr, Woodgate, R. & Lawrence, C. W. Substitution of *mucAB* or *rumAB* for *umuDC* alters the relative frequencies of the two classes of mutations induced by a site-specific T-T cyclobutane dimer and the efficiency of translesion DNA synthesis. *J. Bacteriol.* **178,** 2559–2563 (1996).
22. Trincao, J. *et al.* Structure of the catalytic core of *S. cerevisiae* DNA polymerase η: implications for translesion DNA synthesis. *Mol. Cell* **8,** 417–426 (2001).
23. Washington, M. T., Prakash, L., Prakash, S. & Yeast, D. N. A. polymerase η utilizes an induced-fit mechanism of nucleotide incorporation. *Cell* **107,** 917–927 (2001).
24. Zhou, B. L., Pata, J. D. & Steitz, T. A. Crystal structure of a DinB lesion bypass DNA polymerase catalytic fragment reveals a classic polymerase catalytic domain. *Mol. Cell* **8,** 427–437 (2001).
25. Silvian, L. F., Toth, E. A., Pham, P., Goodman, M. F. & Ellenberger, T. Crystal structure of a DinB family error-prone DNA polymerase from *Sulfolobus solfataricus*. *Nature Struct. Biol.* **8,** 984–989 (2001).
26. Otwinowski, Z. & Minor, W. Processing of X-ray diffraction data collected in oscillation mode. *Methods Enzymol.* **276,** 307–326 (1997).
27. Brünger, A. T. *et al.* Crystallography and NMR system: a new software suite for macromolecular structure determination. *Acta Crystallogr. D* **54,** 905–921 (1998).
28. Jones, T. A., Zou, J.-Y. & Cowan, S. W. Improved methods for building models in electron density maps and the location of errors in these models. *Acta Crystallogr. A* **47,** 110–119 (1991).
29. Vassylyev, D. G. *et al.* Atomic model of a pyrimidine dimer excision repair enzyme complexed with a DNA substrate: structural basis for damaged DNA recognition. *Cell* **83,** 773–782 (1995).
30. Cohen, G. E. ALIGN: a program to superimpose protein coordinates. *J. Appl. Crystallogr.* **30,** 1160–1161 (1997).

Supplementary Information accompanies the paper on **www.nature.com/nature**.

Acknowledgements We thank R. Craigie and D. Leahy for critical reading of the manuscript.

Competing interests statement The authors declare that they have no competing financial interests.

Correspondence and requests for materials should be addressed to W.Y. (Wei.Yang@nih.gov). Coordinates have been deposited in the Protein Data Bank under accession codes 1PM0 and 1PM8.